Charge carrier and exciton dynamics in $LaBr_3:Ce^{3+}$ scintillators: Experiment and model

G. Bizarri* and P. Dorenbos
Faculty of Applied Sciences, Delft University of Technology, Mekelweg 15, 2629JB Delft, The Netherlands
(Received 30 October 2006; revised manuscript received 19 February 2007; published 14 May 2007)

The scintillation yield and decay time of $LaBr_3$ doped with 0.2%, 0.5%, and 5% cerium were studied between 80 K and 600 K. $LaBr_3:5\%Ce^{3+}$ on a photomultiplier tube shows at 300 K a very high scintillation yield of 22 800 photoelectrons per MeV (64 000 photons per MeV) with a decay time of 16 ns. At 600 K the yield decreases by ≃15%. The scintillation yield of $LaBr_3:0.2\%Ce^{3+}$ is 19 800 photoelectrons per MeV (56 000 photons per MeV) at 300 K with a decrease by ≃50% at 600 K and a main scintillation decay time around 30 ns. The appearance of slow components in the Ce emission indicates a relatively slow energy transfer from the host crystal to Ce. The presence or absence of slow components depends on both concentration and temperature. The results are analyzed and interpreted with a model that comprises prompt charge carrier trapping by Ce and delayed excitation of Ce by means of thermally activated transport of self-trapped exciton defects. The results of the study provide detailed information on the scintillation mechanism. Besides presenting experimental data, the different energy transfer processes are quantified.

DOI: 10.1103/PhysRevB.75.184302 PACS number(s): 78.55.Hx, 29.40.Mc, 78.47.+p, 29.30.Kv

I. INTRODUCTION

Cerium doped $LaBr_3$ crystals possess excellent scintillation properties that excite the γ-ray detection community leading to much increased activity in the development of new detection instruments for medical, industrial, security, and space exploration purposes. The invent of $LaBr_3:Ce^{3+}$ is recent and there is still much to learn about these new scintillators. Scintillation properties were presented in various papers[1–6] revealing a strong Ce concentration and temperature dependence. However, neither a detailed investigation on the relation between concentration, temperature, and scintillation properties nor a detailed investigation of the scintillation mechanism was performed.

In our previous work, we proposed a model for the scintillation mechanism of $LaBr_3:0.2\%Ce^{3+}$.[7] We found a competition between different energy and charge carrier transfer processes from the ionization track to Ce that depends on temperature. The prompt trapping of free holes and free electrons by Ce leads to a temperature independent scintillation response governed by the intrinsic lifetime of the emitting $5d$ state of Ce. A thermally activated energy transfer from self-trapped excitons (STEs) to Ce leads to a slow scintillator response that depends on STE lifetime, Ce concentration, and temperature.

In this work, detailed studies on Ce doped $LaBr_3$ are presented. Emission, scintillation yield, and decay time profiles were recorded between 80 K and 600 K with 662 keV γ-ray excitation on samples with 0.2%, 0.5%, and 5% Ce. A dedicated new experimental facility was constructed for the very hygroscopic single crystals with high sensitivity and good reproducability. The decay time profiles are analyzed and fitted with a model that contains energy and charge carrier transfer processes. The data and the model provide us with detailed insight in the scintillation processes in the 1 ns to 1 μs time scale.

II. EXPERIMENT

For this study we used $LaBr_3$ crystals with a Ce concentration of 0.2%, 0.5%, and 5%. For the room temperature (RT) measurements about 10 mm^3 large samples were used while for measurements as functions of temperature crystals with sizes ranging from 0.1 to 0.5 cm^3 were used.

Pulse height spectra at RT were recorded in a dry box with a Hamamatsu R1791 photomultiplier tube (Quartz version of Hamamatsu R878 PMT) connected to a homemade preamplifier, an Ortec 672 spectroscopic amplifier, and an Ortec AD114 CAMAC analog to digital converter. The PMT high voltage was kept at −600 V. The sample was placed without optical coupling on top of the PMT. For efficient collection of scintillation light, the samples were covered with several layers of ultraviolet-reflecting Teflon tape (PTFE tape). The yield of the scintillator, i.e., the number of photons detected by the PMT and expressed in photoelectrons per MeV of absorbed γ energy, was determined by comparing the peak position of the photopeak in the pulse height spectrum with that of the single photoelectron peak. To obtain the absolute light yield in photons per MeV, Eq. (1) was used,[8]

$$Y_{\mathrm{ph}} = Y_{\mathrm{phe}} \frac{1 - R_{\mathrm{eff}}}{R_{\mathrm{PTFE}} \mathrm{QE}_{\mathrm{eff}}}, \tag{1}$$

where $\mathrm{QE}_{\mathrm{eff}}$ and R_{eff} are, respectively, the effective quantum efficiency and effective reflectivity of the R1791 PMT photocathode. The calculated values are 28.7% and 20% for $\mathrm{QE}_{\mathrm{eff}}$ and R_{eff}, respectively. The estimated value of PTFE package reflection (R_{PTFE}) is 0.98. The energy resolution [fullwidth at half-maximum (FWHM) over peak position] was obtained from fitting the 662 keV photopeak.

An x-ray tube with Cu anode operating at 40 kV and 25 mA was used to generate x-ray excited luminescence. The spectra were recorded with an ARC VM504 monochromator (blazed at 300 nm, 1200 grooves/mm) and a Hamamatsu R323 photomultiplier tube (HV −1000 V). The spectra were corrected for the wavelength dependence of the photodetector quantum efficiency as well as for the monochromator transmission. X-ray excited luminescence measurements

were performed between 100 and 600 K using a Janis liquid nitrogen bath cryostat.

For temperature dependent measurements, we constructed a setup to record scintillator events under ^{137}Cs γ-ray excitation (7.4 MBq).[6] The samples are fixed at the bottom of a paraboliclike stainless steel reflector. Both are mounted onto the cold finger of a liquid nitrogen bath cryostat. The sample with the reflector face a photomultiplier tube situated outside the cryostat, which collects nearly all the scintillation light. For the pulse height measurements, the output of that PMT (XP2020Q at −2300 V bias) is integrated via a homemade preamplifier, and a spectroscopic amplifier (Ortec 572). For recording decay curves covering four orders of magnitude in scintillation intensity, the same PMT acts as the start PMT. A hole in the back of the reflector allows a few of the scintillation photons to reach a second PMT (XP 2020Q at −2400 V) acting as the stop PMT. An interference filter in front of this PMT selects the 360 nm Ce emission. The electronic part of the setup is identical to the conventional delayed-coincidence method. LeCroy 934 Constant fraction discriminators (CFDs) and a LeCroy 4208 time to analog converter (TAC) were used.

$LaBr_3$ is very sensitive to moistening even under vacuum conditions. To prevent moistening, we made special precautions. For the room temperature measurement, the experiments were performed inside a dry box with a moisture content less than 1 part per million. For the temperature dependent measurements, the vacuum chamber and the cryostat without sample are baked at 400 K for 2 days. During the baking process all the water is removed from the experimental setup. The pressure is less than 10^{-7} mbar. The sample chamber with cryostat is then vented inside the dry box and inside the dry box the sample is mounted onto the cold finger of the cryostat.

III. SCINTILLATION PROPERTIES

In this section, we will first present x-ray excited emission spectra that will reveal characteristic Ce^{3+} emission together with a broad band lower energy emission which we later will identify as due to so-called self-trapped excitons. Spectra recorded as a function of temperature will reveal an anticorrelation between Ce^{3+} emission intensity and STE emission intensity. Next, γ-ray excited scintillation light yield is determined as a function of temperature and concentration. The absolute light yield turns out to be consistent with the integrated x-ray emission intensity. Finally, the γ-ray scintillation decay profiles are presented as a function of concentration and temperature.

A. X-ray excited emission spectra

X-ray excited emission spectra of $LaBr_3:0.2\%$, 0.5%, and $5\%Ce^{3+}$ at 125 K are shown in Fig. 1(a). Spectra are normalized to each other at 350 nm. Also depicted for the same temperature are the spectra of $LaCl_3:0.5\%Ce^{3+}$ [Fig. 1(b)], and of pure $LaBr_3$ and $LaCl_3$ [Fig. 1(c)]. For all the cerium doped samples, double peaked $5d \rightarrow 4f$ cerium emission is observed. The maxima are located at 355 nm and

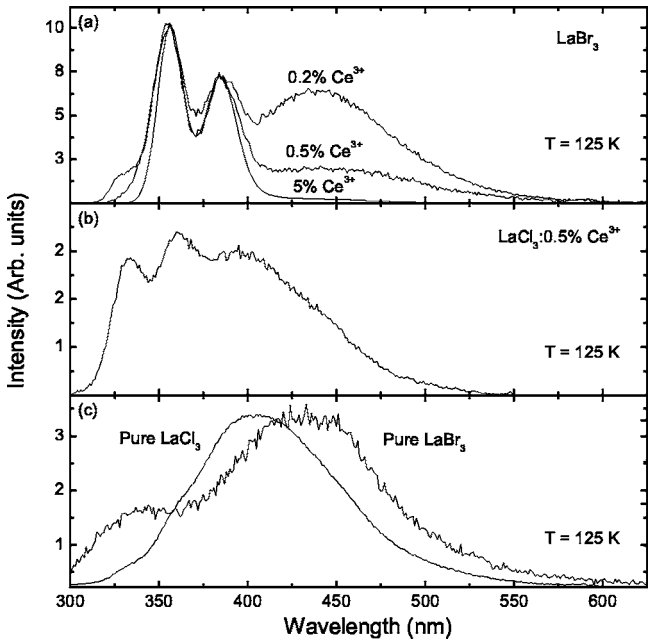

FIG. 1. X-ray excited emission spectra recorded at 125 K (a) of $LaBr_3:0.2\%$, 0.5%, and $5\%Ce^{3+}$, (b) of $LaCl_3:0.5\%Ce^{3+}$, (c) of pure $LaBr_3$ and $LaCl_3$.

385 nm for the bromide, and at 335 nm and 365 nm for the chloride crystals. In addition, a broad emission band is present on the long wavelength side of the Ce^{3+} doublet, peaking at 440 nm for the bromide and 400 nm for the chloride crystals [Figs. 1(a) and 1(b)]. These same emissions are also observed for the pure compounds in Fig. 1(c).

Figure 1(a) shows that when the cerium concentration is raised in $LaBr_3$, the intensity of the broad band relative to the cerium emission decreases. The wavelength scale was transformed to an energy scale and spectra were fitted with three Gaussian-shaped bands. From these fits, the contributions of the Ce^{3+} and of the broad band emissions to the total emission were determined. The contribution of the broad band decreases from 70% to 37% to 8% for a concentration of 0.2%, 0.5%, and 5%, respectively.

Figure 2 shows the temperature dependence of x-ray excited emission for $LaBr_3:0.2\%Ce^{3+}$ from 125 to 200 K in temperature steps of 25 K. The characteristic doublet structure of the cerium emission is present as well as the lower energy broad band emission. As the temperature rises, the Ce^{3+} luminescence intensity is enhanced at the expense of the broad band luminescence intensity.

Figure 3 shows the temperature dependence between 125 K and 600 K of Ce^{3+}, broad band, and total luminescence intensity in $LaBr_3:0.2\%Ce^{3+}$, derived from x-ray induced emission spectra. The total light yield decreases with increasing temperature. At 125 K, the emission is dominated by the broad band. With increasing temperature, the Ce^{3+} emission increases at the expense of the broad band emission. Above 250 K, almost all emission is due to Ce^{3+}. Similar results were obtained with $LaBr_3:0.5\%$ and 5% Ce^{3+} samples.

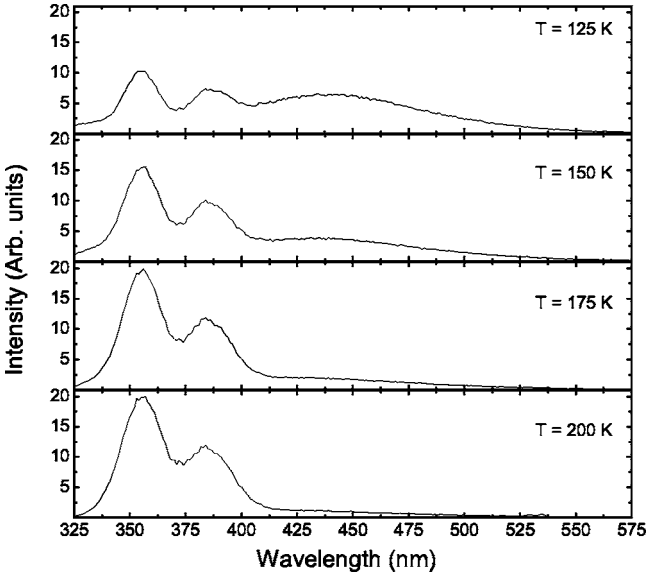

FIG. 2. Temperature dependence of x-ray excited emission spectra of $LaBr_3:0.2\%Ce^{3+}$ recorded at 125, 150, 175, and 200 K.

B. Light output

Figure 4 shows pulse-height spectra of $LaBr_3:0.2$, 0.5%, and $5\%Ce^{3+}$ recorded with a shaping time of 10 μs at room temperature under ^{137}Cs 662 keV γ-ray excitation. Derived scintillation yields and energy resolutions from the 662 keV total absorption peak recorded with different shaping times are compiled in Table I.

The highest yield of 22 800 photoelectrons per MeV (64 000 photons per MeV) was measured with a shaping time of 10 μs for $LaBr_3:5\%Ce^{3+}$. The yield decreases to 21 500 and 19 800 photoelectron per MeV (60 500 and 56 000 photons per MeV, respectively) for 0.5% and 0.2% Ce. The yield at fixed Ce concentration does not change much with shaping time indicating that an electronic integration time of 0.5 μs is long enough to record the entire scintillation pulse at room temperature. The energy resolution is around 3%.

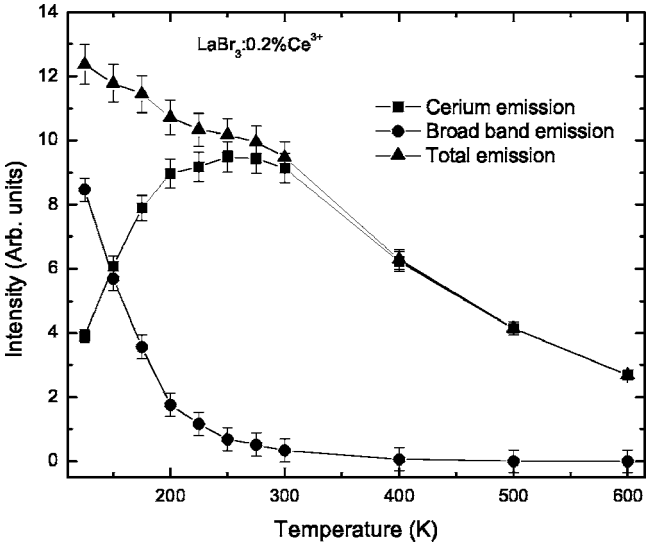

FIG. 3. Temperature dependence of the light yields of Ce^{3+}, broad band, and total luminescence in $LaBr_3:0.2\%Ce^{3+}$, derived from x-ray induced emission spectra. Solid lines are shown to guide the eye.

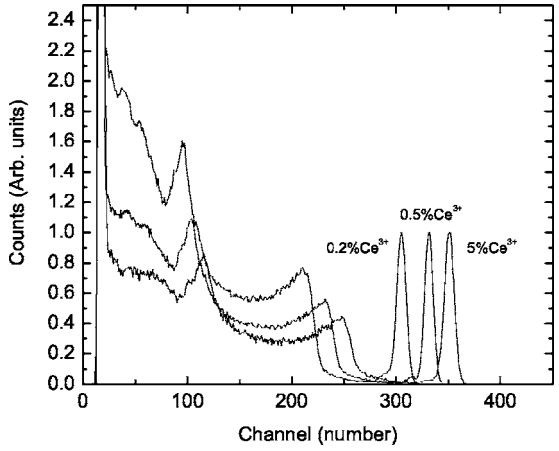

FIG. 4. ^{137}Cs source scintillation pulse height spectra measured with $LaBr_3:Ce^{3+}$. The 662 keV total absorption peaks are present between channel 300 and 350.

Figure 5 shows the scintillation yields of $LaBr_3:0.2\%$, 0.5%, and $5\%Ce^{3+}$ as a function of temperature recorded under ^{137}Cs 662 keV γ-ray excitation with a shaping time of 10 μs. The maximum is reached at 200 K for all three samples. Above 200 K, the yield decreases with decreasing Ce concentration and increasing temperature. At 600 K, the loss reaches about 50%, 25%, and 15% for $LaBr_3:0.2\%$, 0.5%, and $5\%Ce^{3+}$, respectively. The temperature dependence for the 0.2% doped crystal is similar to the one observed under x-ray excitation in Fig. 3. Below 200 K, the yield decreases with decreasing temperature. Actually this decrease is an artefact of the experiment, i.e., the ballistic deficit. Part of the scintillation pulse at low temperature and small Ce concentration becomes slower than the electronic shaping time used for themeasurement, and then that part of the scintillation pulse does not contribute to the pulse height. When the light yield is derived from x-ray emission spectra (Fig. 3), the ballistic deficit does not occur.

C. Scintillation time profiles

Figures 6–8 show the temperature dependence of γ-ray excited scintillation response for $LaBr_3:0.2\%$, 0.5%, and $5\%Ce^{3+}$ between 80 K and 600 K. On the left-hand side the long time range response is presented in a log-log representation. The right-hand side shows the response at a short time range in a log-lin representation. This latter representation allows a better display of the initial rise of the scintillation response.

Clear trends in $LaBr_3$ scintillation response can already be observed. Well below 400 K, 300 K, and 200 K for $LaBr_3:0.2\%$, 0.5%, and $5\%Ce^{3+}$, respectively, the decay curves are composed of a few tens of nanoseconds fast exponentially decaying component with in addition a much slower component sometimes extending into the microsecond region. When the temperature increases the slow com-

TABLE I. Scintillation yield Y in photoelectrons per MeV and energy resolution R derived from ^{137}Cs 662 keV γ-ray pulse height spectra of $LaBr_3:Ce^{3+}$ with 0.2%, 0.5%, and 5% Ce at RT and recorded with different shaping times (ST).

	Scintillation yield Y (photoelectrons/MeV)			R (%)
Sample	ST=0.5 μs	ST=3 μs	ST=10 μs	
$LaBr_3:0.2\%Ce^{3+}$	18300	19450	19800	3.4
$LaBr_3:0.5\%Ce^{3+}$	20050	21350	21500	2.9
$LaBr_3:5\%Ce^{3+}$	21050	22400	22800	3

ponent gradually fastens and eventually merges with the fast one. The merging temperature decreases with increasing Ce concentration. Above 400 K, 300 K, and 200 K for $LaBr_3:0.2\%$, 0.5%, and $5\%Ce^{3+}$ both components are indistinguishable. At the merging temperature the decay curve, especially at low Ce concentration of 0.2% in Fig. 6(b), develops a slow rise in the first 10 ns of the pulse.

To further analyze the data and to translate it into a general scintillation mechanism for $LaBr_3:Ce$, the measured decay profiles were fitted with a set of equations that reflect different energy and charge carrier transfer processes from the ionization track to Ce.

IV. THE SCINTILLATION MODEL

In the past, several scintillation mechanisms for Ce doped LaX_3 were proposed.[1,2,9] Due to a lack of accurate experimental data on yield and decay time as functions of temperature and concentration, the suggested models could only provide a qualitative description of the scintillation processes. This work provides the required data as a function of four important parameters; wavelength, temperature, Ce concentration, and time.

We will first argue that STE are responsible for the broad emission band at 450 nm in Fig. 1 and that they play an important role in the scintillation process. Then a mathemati-

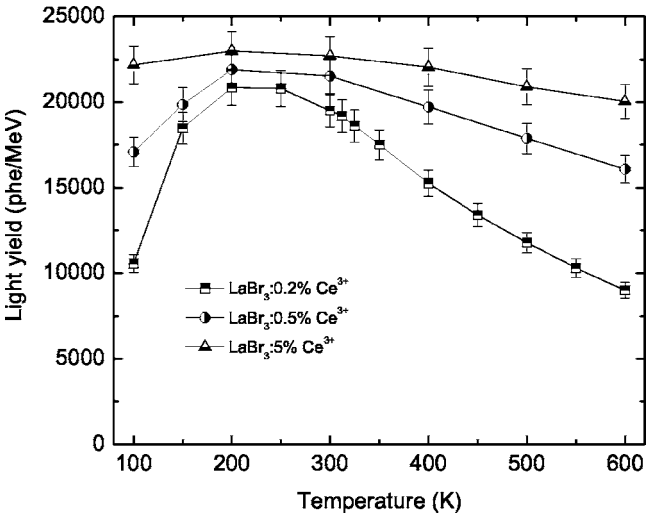

FIG. 5. Temperature dependence of $LaBr_3:0.2\%$, 0.5%, and $5\%Ce^{3+}$ scintillation yield. Solid lines are shown to guide the eye.

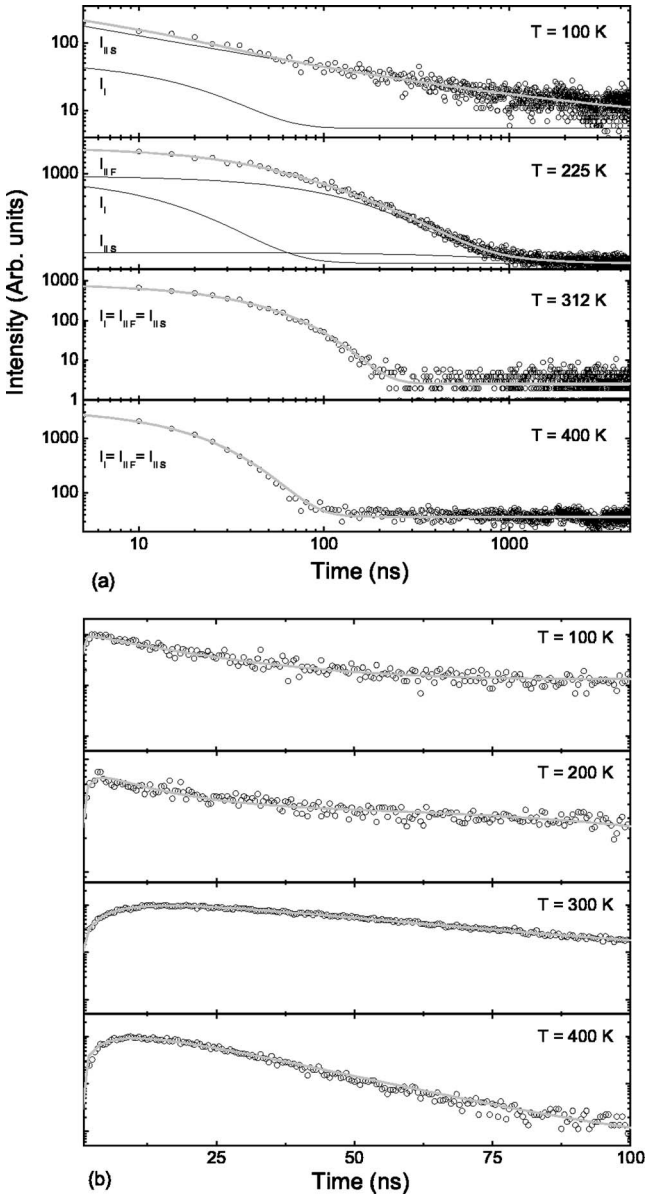

FIG. 6. Temperature dependence of Ce scintillation time profiles in $LaBr_3:0.2\%Ce^{3+}$ (a) for a measurement recorded on a long time domain in a log-log scale representation and (b) for one recorded on a short time domain in a log-lin scale representation. Curves labelled I_I, $I_{II\,F}$, $I_{II\,S}$ are the fitted decay components.

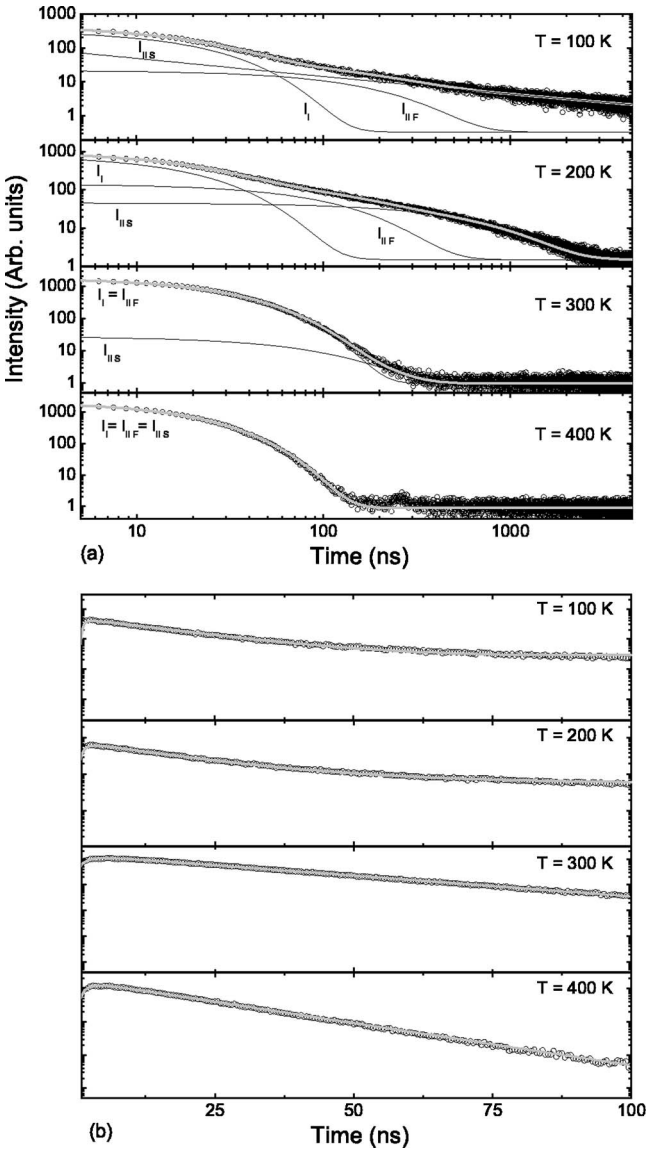

FIG. 7. Temperature dependence of Ce scintillation time profiles in $LaBr_3:0.5\%Ce^{3+}$ (a) for a measurement recorded on a long time domain in a log-log scale representation and (b) for one recorded on a short time domain in a log-lin scale representation. Curves labelled I_I, $I_{II\,F}$, $I_{II\,S}$ are the fitted decay components.

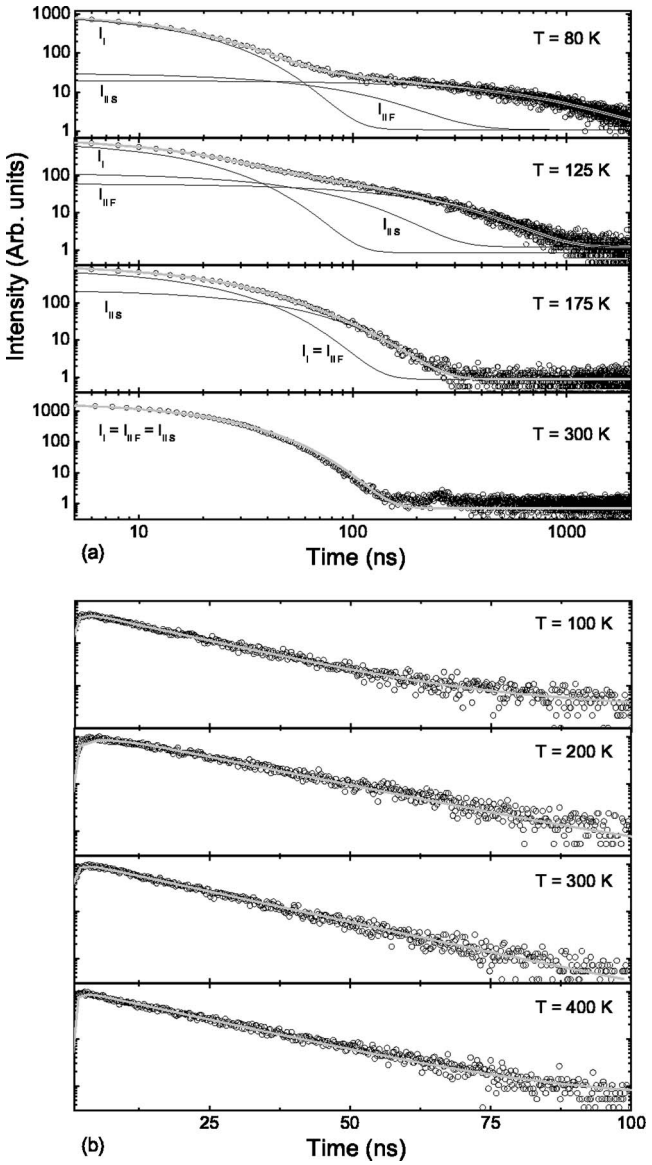

FIG. 8. Temperature dependence of Ce scintillation time profiles in $LaBr_3:5\%Ce^{3+}$ (a) for a measurement recorded on a long time domain in a log-log scale representation and (b) for one recorded on a short time domain in a log-lin scale representation. Curves labelled I_I, $I_{II\,F}$, $I_{II\,S}$ are the fitted decay components.

cal model based on rate equations is formulated. Finally the model is applied to the decay time spectra and the relevant parameters are derived.

A. The model

We distinguish two main energy and charge carrier transfer mechanisms that lead to Ce emission in $LaBr_3$: the sequential capture of charge carriers by Ce^{3+} and the thermally activated energy transfer from STEs to cerium ions.

Process I is the prompt capture, i.e., faster than 1 ns, of a free hole (h^+) and a free electron (e^-) from the ionization track by Ce leading to $4f$-$5d$ excitation and followed by fast $5d$-$4f$ emission.

The prompt capture of charge carriers by Ce^{3+} is revealed by the fast time response component observed in Figs. 6–8. The decay of the fast component agrees with the 16 ± 2 ns cerium intrinsic lifetime in $LaBr_3$ recorded under optical excitation.[5] This prompt transfer leads to part of the $5d\rightarrow4f$ cerium emission in Fig. 1(a).

Process II is a thermally activated energy transfer from self-trapped excitons to Ce. The doublet Ce emission, the broad band lower energy emission, and the anticorrelation between them with the increase of temperature in Figs. 1–3 are very similar to features observed for $LaCl_3:Ce^{3+}$.[1,2]

In $LaCl_3$, the presence of two types of STEs was established by x-ray excited electron-paramagnetic-resonance spectra.[10] Both types correspond to an *out-of-plane* self-trapped exciton formed by two nearest Cl^- neighbors.[10] One

TABLE II. Results from fitting the scintillation model to the Ce scintillation decay profile of $LaBr_3$:0.2%,0.5%, and 5% Ce^{3+}.

		Components				
		Process I	Process II			
			Fast process		Slow process	
Sample	Temperature (K)	τ_{Ce} (ns)	τ_E (ns)	τ_D (ns)	s	τ_{T2} (ns)
$LaBr_3$:0.2% Ce^{3+}	100	18(1.3%)		≃1	0.5(98.7%)	
$LaBr_3$:0.2% Ce^{3+}	225	19(11.4%)	236(69.9%)	1.5		1120(18.7%)
$LaBr_3$:0.2% Ce^{3+}	300		35(100%)	8.75		
$LaBr_3$:0.2% Ce^{3+}	400		16(100%)	6.59		
$LaBr_3$:0.2% Ce^{3+}	500	16(100%)		≃1		
$LaBr_3$:0.2% Ce^{3+}	600	16(100%)		≃1		
$LaBr_3$:0.5% Ce^{3+}	100	18(21.2%)	140(11.5%)	≃1	0.54(67.3%)	
$LaBr_3$:0.5% Ce^{3+}	200	18(26.1%)	96(26.6%)	1.2		550(47.3%)
$LaBr_3$:0.5% Ce^{3+}	300		27(95.8%)	2.2		80(4.2%)
$LaBr_3$:0.5% Ce^{3+}	400	16(100%)		≃1		
$LaBr_3$:0.5% Ce^{3+}	500	16(100%)		≃1		
$LaBr_3$:0.5% Ce^{3+}	600	18(100%)		≃1		
$LaBr_3$:5% Ce^{3+}	80	15(42%)	140(11%)	≃1		710(47%)
$LaBr_3$:5% Ce^{3+}	125	16(38%)	75(28%)	≃1		267(34%)
$LaBr_3$:5% Ce^{3+}	175	18(56.9%)	43(43.1%)	≃1		
$LaBr_3$:5% Ce^{3+}	300	16(100%)		≃1		
$LaBr_3$:5% Ce^{3+}	400	16(100%)		≃1		
$LaBr_3$:5% Ce^{3+}	500	18(100%)		≃1		
$LaBr_3$:5% Ce^{3+}	600	21(100%)		≃1		

of the STEs was directly related to the broad band emission centered at 400 nm observed for doped and pure $LaCl_3$ [Figs. 1(b) and 1(c)]. By analogy, we attribute the broad band emission centered at 440 nm in $LaBr_3$ [Figs. 1(a) and 1(c)] also to an excitonic emission.[11] The transfer from STEs to Ce^{3+} is revealed by the temperature dependence of the Ce and STE emissions intensity in Figs. 2 and 3. The anticorrelation between Ce^{3+} and STE luminescence shows that the energy located on STEs ends at the cerium ions. This anticorrelation has also been observed in $LaCl_3$:0.57% Ce^{3+} by Guillot-Noël *et al.*[1] and in K_2LaCl_5:0.23% Ce^{3+} by van't Spijker *et al.*[17]

A STE to Ce^{3+} energy transfer is also consistent with the concentration and temperature dependences observed in Figs. 1, 2, and 5. The free charge carriers compete between the creation of an excited cerium ion and the formation of a STE which leads to a decrease of the STE emission when the Ce concentration rises, see Fig. 1. The thermal quenching of STE emission explains the light loss observed above 300 K in Figs. 3 and 5. The higher contribution of STE emission at low Ce concentration, see Fig. 1(a), enhances the energy loss at temperature between 300 K and 600 K in Fig. 5.

Further evidence of a thermally activated energy transfer is the risetime observed in the time response of Ce emission. For $LaBr_3$:0.2% at 300 and 400 K the decay time presents a risetime of 8.75 and 6.6 ns, respectively, see Fig. 6 and Table II. At 300 K, $LaBr_3$:0.5% Ce time response shows also a risetime with a value of 2.2 ns, see Fig. 7 and Table II.

B. Mathematical description

Using rate equations and solving them, the different processes of the scintillation mechanism can be described mathematically.

Process I: The sequence of events is illustrated by Eqs. (2)–(4), and Fig. 9,

$$Ce^{3+} + h^+ \rightarrow Ce^{4+}, \tag{2}$$

$$Ce^{4+} + e^- \rightarrow Ce^{3+*}, \tag{3}$$

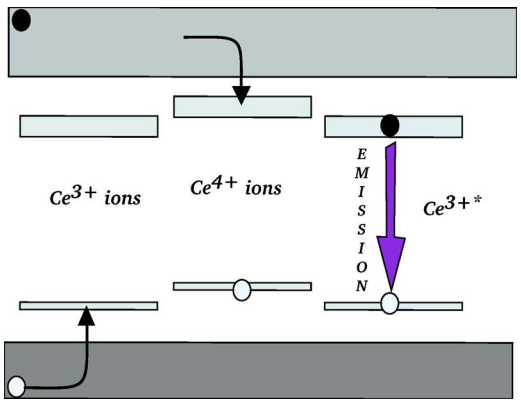

FIG. 9. (Color online) Model of scintillation illustrating the sequential capture of primary charge carriers by Ce^{3+}.

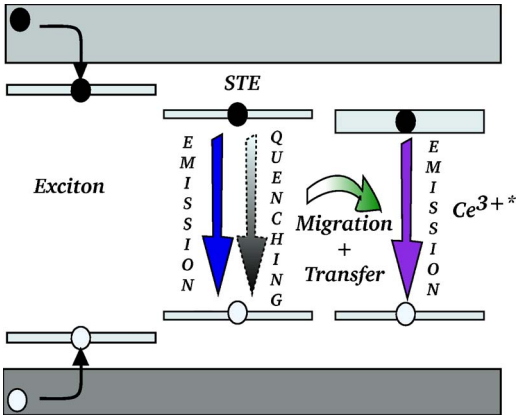

FIG. 10. (Color online) Model of scintillation illustrating process II; creation of STEs and energy transfer from STEs to cerium.

$$Ce^{3+*} \rightarrow Ce^{3+} + h\nu. \tag{4}$$

It is also possible that prior to Eq. (2) the hole is first trapped by two bromine anions to form a so-called V_k center which then migrates towards a Ce^{3+} to form eventually Ce^{4+}. The scintillation profile $I_I(t)$ of process I is given by

$$I_I(t) = Ae^{-t/\tau_{Ce}}, \tag{5}$$

which is a single exponentially decaying function with τ_{Ce} the lifetime of the Ce^{3+} $5d$ state.

Process II: The sequence of events is illustrated by Eqs. (6) and (9) and by Fig. 10,

$$2Br^- + h^+ \rightarrow V_k, \tag{6}$$

$$V_k + e^- \rightarrow \text{STE} \tag{7}$$

$$Ce^{3+} + \text{STE} \rightarrow Ce^{3+*}, \tag{8}$$

$$Ce^{3+*} \rightarrow Ce^{3+} + h\nu. \tag{9}$$

Prior to STE creation a hole is trapped by two bromine anions to form a V_k center that subsequently traps an electron to form a STE.[10]

This alone appears not sufficient to fit or reproduce all decay curves in Figs. 6–8. We need to introduce two different STE→Ce transfer processes. Tentatively we associate one process with thermally activated migration of STEs through the lattice towards Ce. This process appears in the scintillation response curves at 100 K for 0.2% and 0.5% doped samples and is referred to as *slow process II*. After the STE has arrived close to a Ce^{3+}, a thermally activated transfer of excitation energy from STE to Ce occurs. This process is referred to as *fast process II*. Both processes are illustrated in Fig. 11. Note that the slow process is always followed by the fast one.

Fast process II is determined by the barrier for energy transfer from an STE in the immediate vicinity of Ce to that Ce ion as illustrated in Fig. 11. This transfer is easily modelled with two coupled rate equations. N_{STE} is the number of STEs located in the surrounding of Ce. The decay rate $\frac{1}{\tau_E}$ of the exciton is equal to $\Gamma_R+\Gamma_Q+\Gamma_{T1}$ with Γ_R, Γ_Q, Γ_{T1} the STE radiative decay rate, the STE thermal quenching rate, and the transfer rate from an STE to Ce, respectively. The rate of change of N_{STE} is given by

$$\frac{dN_{STE}}{dt} = -(\Gamma_R + \Gamma_Q + \Gamma_{T1})N_{STE}. \tag{10}$$

N^*_{Ce} is the number of Ce $5d$ states excited via energy transfer from STEs. By taking into account the radiative decay rate $\Gamma_{Ce}=\frac{1}{\tau_{Ce}}$, the rate of change of N^*_{Ce} is given by

$$\frac{dN^*_{Ce}}{dt} = \Gamma_{T1}N_{STE} - \Gamma_{Ce}N^*_{Ce}. \tag{11}$$

Solving rate Eqs. (10) and (11) gives

$$N_{STE} = N_{STE_0}e^{-t/\tau_E}, \tag{12}$$

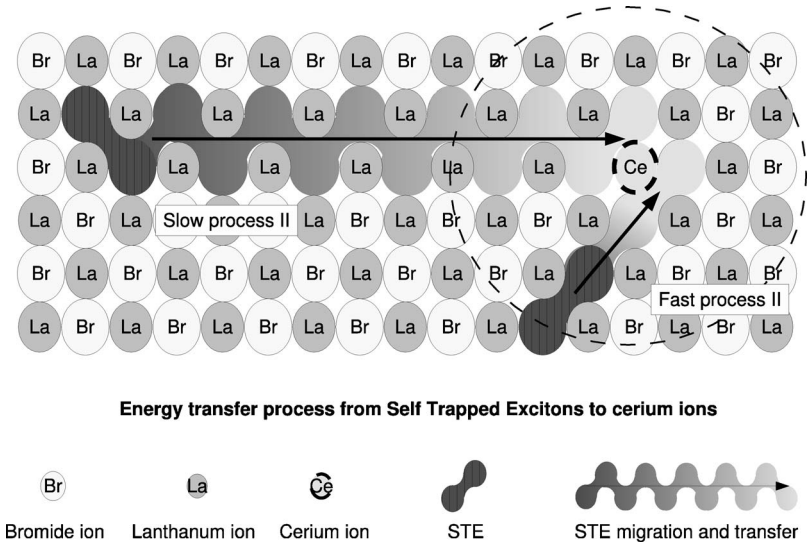

FIG. 11. Model of scintillation illustrating two different STE to cerium transfer processes.

$$N^*_{Ce} = \frac{N_{STE_0}\Gamma_{T1}}{\frac{1}{\tau_E} - \frac{1}{\tau_{Ce}}}(e^{-t/\tau_{Ce}} - e^{-t/\tau_E}), \quad (13)$$

with N_{STE_0} the number of STEs formed at $t=0$.

When $\tau_E \ll \tau_{Ce}$, Eq. (13) becomes equivalent to Eq. (5). The contribution of *Process I* and *fast process II* to the scintillation response cannot be distinguished anymore. Already when $\tau_E \simeq \tau_{Ce}$ it appears impossible to reliably analyze the scintillation response with a combination of Eq. (5) and Eq. (13). We therefore, but also in order not to restrict the fitting too much with the idealized theoretical expressions of Eq. (5) and Eq. (13), have chosen to replace Eq. (13) with the more general equation

$$I_{IIF}(t) = B(e^{-t/\tau_E} - e^{-t/\tau_D}). \quad (14)$$

The cerium scintillation time profile on the long time scale is given by an exponential decay governed by the decay time τ_E of STEs.

Slow process II results from the thermally activated migration of STEs to Ce as illustrated in Fig. 11. When the migration rate Γ_{T2} from an STE located far from Ce towards a Ce ion is much slower than the Ce decay rate Γ_{Ce} then Eq. (14) reduces to

$$I_{IIS}(t) = Ce^{-t/\tau_{T2}} \quad (15)$$

and an exponentially decaying slow component will be present in the scintillation decay profile. However, our results reveal that for low Ce concentrations and low temperature the scintillation profile cannot be fitted with an exponentially decaying function. Instead it appears to decay as a power law with time

$$I_{IIS}(t) = Dt^{-s} \quad \text{with } s \simeq 0.5. \quad (16)$$

The physical processes behind a power-law relationship are complex and may involve several stages.[12–16] In general such relationship is expected and observed when there is migration in a disordered medium. Tunneling, diffusion, or percolation through a lattice with a distribution of site-to-site tunneling probabilities or energy barriers, and with a random distribution of defects often result in power-law-like diffusion rates. At low temperature ($\simeq$100 K) and at low Ce concentration ($<0.5\%$), this energy transfer appears dominant in $LaBr_3$. At higher temperature, the slow scintillation decay component is described best by an exponential decay, according to Eq. (15). Eventually, the migration rate Γ_{T2} becomes much higher than the transfer rate Γ_{T1} and *slow process II* merges into *fast process II*.

C. Fitting parameters

Based on Eqs. (5) and (14)–(16), the Ce scintillation decay profiles at 360 nm were fitted over all the temperature ranges. In Figs. 6–8, we plotted for each temperature the experimental data (open circle) and the result of the fitting process (gray curve). In Figs. 6(a), 7(a), and 8(a), the fit is decomposed into contributions from *process I* (I_I), *fast process II* (I_{IIF}), and *slow process II* (I_{IIS}). The values for the fitting parameters, τ_{Ce}, τ_E, τ_D, s, and τ_{T2}, are compiled in Table II. The numbers within parentheses correspond with the relative contribution to the Ce emission at 360 nm coming from *process I* (I_I), *fast process II* ($I_{II\ F}$), and *slow process II* ($I_{II\ S}$). Each contribution is calculated from integration of the fitted decay components.

V. DISCUSSION

Almost all decay curves in Figs. 6–8 reveal a fast component with a decay time of 17 ± 2 ns, see Table II. This value is close to the 16 ± 2 ns intrinsic lifetime of the emitting Ce $5d$ state measured for $LaBr_3$:Ce under optical excitation.[5] It does not change with temperature or Ce concentration. The same was observed under optical excitation of $LaBr_3$:Ce. The temerature stability of Ce emission was explained by a large energy difference between the cerium $5d$ state and the conduction band.[5,11]

The probability of prompt capture and therewith the contribution of the fast component to the total yield increases with Ce concentration. At 100 K, the fast component contribution increases from 1% to $\simeq$40% from $LaBr_3$:0.2% Ce^{3+} to $LaBr_3$:5% Ce^{3+}, see Table II.

The prompt capture probability of charge carriers by Ce may also depend on temperature because the creation rate of STEs, see Eqs. (5) and (6), and the hole capture rate by Ce^{3+}, see Eq. (2), are possibly related with thermally activated migration of V_k centers. Between 100 and 300 K the contribution of the fast component to the Ce emission does not change significantly for 0.5% and 5% doped $LaBr_3$. However, at concentration of 0.2% Table II shows a 10 times increased prompt capture probability when temperature increases from 100 to 225 K.

Above 400, 300, and 200 K, the contribution of the fast component to the total yield reaches 100% for $LaBr_3$:0.2% Ce^{3+}, $LaBr_3$:0.5% Ce^{3+}, and $LaBr_3$:5% Ce^{3+}, respectively. This is fully attributed to the increase of Γ_{T1} (*fast process II*) and Γ_{T2} (*slow process II*). For $LaBr_3$:0.5% Ce^{3+} τ_E decreases from 140 ns to 27 ns and τ_{T2} from a value higher than 550 ns to 80 ns between 100 and 300 K, respectively. Above 300 K, τ_E and τ_{T2} become faster than τ_{Ce}. The STE$\rightarrow$Ce transfer is then faster than the lifetime of Ce, and scintillation components due to process II merge together with that from process I. The resulting time response is fully governed by the intrinsic Ce emission decay time.

Because Γ_{T2} increases faster than Γ_{T1} with increasing temperature, we observe a gradual shift in the energy transfer from the *slow process II* mechanism to the *fast process II* mechanism. For $LaBr_3$:0.2% Ce^{3+} we observe first a power-law decay time component at 100 K that turns into a combination of a fast and slow exponential component at 225 K. At room temperature the scintillation profile is well described by Eq. (14) of the *fast process II*; a clear risetime is observed in Fig. 6. At 300 K for both $LaBr_3$:0.2% and 0.5% Ce^{3+}, *slow process II* is not observed anymore. The *fast process II* becomes the rate determining energy transfer mechanism hiding the contribution coming from *process I*.

In this work we used Eqs. (5), (15), and (16) to fit the scintillation decay curves measured at 360 nm as functions

of temperature and Ce concentration. Excellent fits providing parameter values that describe the various scintillation processes are obtained. Process I describes a 17 ± 2 ns Ce^{3+} emission component. Fast process II describes a combination of Ce^{3+} and STE emission. The ratio of Ce^{3+} to STE emission from fast process II depends on the unknown parameters Γ_R, Γ_Q, and Γ_{T1} that determine $\frac{1}{\tau_E}$ in Eqs. (12) and (13). Although these parameters are not yet known as functions of temperature and concentration, all the main features in the emission and scintillation intensity in Figs. 1–3, and Fig. 5 are already explained qualitatively by our scintillation model and the parameter values in Table II.

The disappearing of the STE emission at 125 K when the concentration increases from 0.2% to 5% in Fig. 1(a) is now attributed to an increase of the transfer rate from STE to Ce to values higher than the radiative lifetime Γ_R of the STE. The same applies to the anticorrelation between STE emission and Ce emission observed in Fig. 2 and Fig. 3 for $LaBr_3:0.2\%Ce$ when the temperature increases from 125 K to room temperature. Again the transfer rate from STE to Ce becomes larger than the radiative decay rate Γ_R of the STE leading to decrease of STE emission and increase of Ce emission. The decrease of the Ce emission with temperature above 300 K in Fig. 3 for $LaBr_3:0.2\%Ce$ is attributed to the thermal quenching rate Γ_Q of the STE that apparently becomes faster than the transfer rate to Ce and the radiative lifetime Γ_R. One now even understands why in Fig. 5 the amount of scintillation quenching at 600 K deceases when the Ce concentration increases from 0.2% to 5%. There are two reasons. First, the smaller part of the total emission is due to energy transfer from STE to Ce, and that is the only part that can be quenched thermally. Second, the thermal quenching of that part is reduced because the transfer rate increases with Ce concentration whereas the thermal quenching rate of the STE is most likely independent on concentration.

In a forthcoming work we intend to use our scintillation model to fit, besides the decay time spectra in Figs. 6–8, simultaneously data on the absolute light yield as in Fig. 5 and data from emission spectra as in Fig. 3. It will provide us with the STE quenching rates and STE to Ce transfer rates as functions of temperature and concentration from which we expect to extract the activation energies for energy transfer and for STE quenching.

VI. CONCLUSION

γ-ray pulse height spectra and scintillation decay time profiles were measured between 80 K and 600 K on samples with 0.2%, 0.5%, and 5% Ce. These data were analyzed with a scintillation model that contains the following energy and charge carrier transfer processes from the ionization track created by a γ particle to Ce:

(i) The prompt sequential capture of the primary charge carriers by Ce.

(ii) Thermally activated energy transfer from self-trapped excitons situated in the close surrounding of a cerium ion to that cerium ion.

(iii) Thermally activated migration of STEs towards Ce followed by energy transfer from STE to Ce. The migration phase may lead to a power-law-like or a slow exponential contribution to the scintillation pulse.

The competition between all those mechanisms determines the scintillation properties as functions of the temperature and Ce concentration. At low Ce concentration and low temperature, STEs are created with high efficiency. Thermally activated STE diffusion to Ce is then the dominant scintillation mechanism. It results in a relatively slow decay component. If the Ce concentration or the temperature increases, the speed of STE energy transfer to Ce increases. At high Ce concentration or high temperature, the transfer rate from STEs to Ce is faster than the Ce lifetime. The scintillation decay profile is then entirely governed by the intrinsic lifetime of Ce. For intermediate cerium concentrations and temperatures, all these mechanisms are present simultaneously and slow and fast components are mixed. The time response of $LaBr_3$ is the result of the competition between those different energy transfer processes.

The combination of accurate scintillation profile measurements and model fitting provides the parameter values of different transfer processes as functions of concentration and temperature.

ACKNOWLEDGMENTS

This work was financed by the Idaho National Engineering and Environmental Laboratory and the U.S. Department of Energy. The authors thank Saint Gobain, Division Crystals and Detectors, Nemours, France for providing the scintillators used in this work.

*Electronic address: g.a.bizarri@tudelft.nl

[1] O. Guillot-Noël, J. T. M. de Haas, P. Dorenbos, C. W. E. van Eijk, K. W. Krämer, and H. U. Güdel, J. Lumin. **85**, 21 (1999).
[2] E. V. D. van Loef, P. Dorenbos, and C. W. E. van Eijk, Appl. Phys. Lett. **79**, 1573 (2001).
[3] E. V. D. van Loef, P. Dorenbos, C. W. E. van Eijk, K. W. Krämer, and H. U. Güdel, Nucl. Instrum. Methods Phys. Res. A **486**, 254 (2002).
[4] E. V. D. van Loef, P. Dorenbos, and C. W. E. van Eijk, J. Phys.: Condens. Matter **15**, 1367 (2003).
[5] G. Bizarri, J. T. M. de Haas, P. Dorenbos, and C. W. E. van Eijk, IEEE Trans. Nucl. Sci. **53**, 615 (2006).
[6] G. Bizarri, J. T. M. de Haas, P. Dorenbos, and C. W. E. van Eijk, Phys. Status Solidi A **203**, R41 (2006).
[7] G. Bizarri and P. Dorenbos, Phys. Status Solidi C **3**, 3434 (2006).
[8] J. T. M. de Haas, P. Dorenbos, and C. W. E. van Eijk, Nucl. Instrum. Methods Phys. Res. A **537**, 97 (2005).
[9] P. Dorenbos, Phys. Status Solidi A **202**, 195 (2005).

[10] U. Rogulis, S. Schweizer, J. M. Spaeth, E. V. D. van Loef, P. Dorenbos, C. W. E. van Eijk, K. W. Krämer, and H. U. Güdel, Radiat. Eff. Defects Solids **157**, 951 (2002).
[11] J. C. van't Spijker, P. Dorenbos, C. W. E. van Eijk, K. W. Krämer, and H. U. Güdel, J. Lumin. **85**, 1 (1999).
[12] T. R. Waite, Phys. Rev. **107**, 463 (1957).
[13] K. Tanimura and N. Itoh, J. Phys. Chem. Solids **42**, 901 (1981).
[14] A. K. Jonscher and A. de Polignac, J. Phys. C **17**, 6493 (1984).
[15] L. A. Dissado, Chem. Phys. Lett. **124**, 206 (1986).
[16] E. V. D. van Loef, P. Dorenbos, and C. W. E. van Eijk, J. Phys.: Condens. Matter **15**, 1367 (2003).
[17] P. Dorenbos, E. V. D. van Loef, A. P. Vink, E. van der Kolk, C. W. E. van Eijk, K. W. Krämer, H. U. Güdel, W. M. Higgins, and K. S. Shah, J. Lumin. **117**, 147 (2006).